Materials Science-Poland, 37(3), 2019, pp. 404-416
http://www.materialsscience.pwr.wroc.pl/
DOI: 10.2478/msp-2019-0043

Deposition time and annealing effects on morphological and optical properties of ZnS thin films prepared by chemical bath deposition

N. CHABOU[1,*], B. BIROUK[1], M.S. AIDA[2], J.P. RASKIN[3]

[1]Renewable Energies Laboratory (LER)/Jijel University, Algeria
[2]Thin Films and Interfaces Laboratory, Constantine University, Algeria
[3]ICTEAM/Université Catholique de Louvain (UCL), Louvain-La-Neuve, Belgium

Nanocrystalline zinc sulfide thin films were prepared on glass substrates by chemical bath deposition method using aqueous solutions of zinc chloride, thiourea ammonium hydroxide along with non-toxic complexing agent trisodium citrate in alkaline medium at 80 °C. The effect of deposition time and annealing on the properties of ZnS thin films was investigated by X-ray diffraction, scanning electron microscopy, optical transmittance spectroscopy and four-point probe method. The X-ray diffraction analysis showed that the samples exhibited cubic sphalerite structure with preferential orientation along ⟨2 0 0⟩ direction. Scanning electron microscopy micrographs revealed uniform surface coverage, UV-Vis (300 nm to 800 nm) spectrophotometric measurements showed transparency of the films (transmittance ranging from 69 % to 81 %), with a direct allowed energy band gap in the range of 3.87 eV to 4.03 eV. After thermal annealing at 500 °C for 120 min, the transmittance increased up to 87 %. Moreover, the electrical conductivity of the deposited films increased with increasing of the deposition time from 0.35×10^{-4} Ω·cm^{-1} to 2.7×10^{-4} Ω·cm^{-1}.

Keywords: *CBD; ZnS; complexing agent; stirring; annealing; free buffer layer*

1. Introduction

Development of materials in form of thin layers is of major interest in a wide range of applications. These thin layers have, in particular, different physicochemical properties from those of bulk materials. Thin films of chalcogenides are semiconductors which have attracted a lot of attention last years because of their remarkable physical properties in opto-electronic applications [1] as well as in solar cells fabrication as a buffer layer. Nowadays, the most often used among these materials is zinc sulfide. ZnS has a large direct band gap of 3.65 eV to 3.7 eV, high refractive index of 2.25 to 2.35, and great exciton binding energy of 40 meV with n-type electrical conductivity. It has been extensively utilized in light emitting devices [2], electroluminescent devices, semiconductor lasers [3], flat panel displays [4], optical sensors [5], phosphors [6], and so on. ZnS thin films have been found valuable as buffer layer in replacement of the harmful CdS in CIGS thin film solar cells.

Different techniques can be used to deposit such material in thin film form, which originate from purely physical or purely chemical processes such as close-spaced vacuum sublimation technique (CSVS) [7], molecular beam epitaxy [8], thermal evaporation [9], successive ionic layer adsorption and reaction (SILAR) [10], RF magnetron sputtering [11], chemical vapor deposition (CVD) [12], electrodeposition [13], spray pyrolysis [14] and flash evaporation technique [15]. The physical properties of the material are strongly dependent on the methods of preparation. We chose the method called CBD as this relatively simple, economical and cost effective process can be carried out at low temperature and pressure. The film can be easily coated on large surfaces. This method allows also deposition of optically smooth, uniform and homogeneous layers. Chemical bath

*E-mail: chabounawel@yahoo.fr

deposition was used to deposit ZnS semiconductors [16]. The quality of the deposited film depends on the bath parameters, such as temperature, time of deposition, concentration of the reactants and the pH of the chemical bath. Recently, thin film solar cells based on chemical bath deposition ZnS (O, OH) buffer layer have achieved an efficiency of 18.6 % [17, 18].

In this work, ZnS thin films were deposited by the chemical bath deposition technique. The thin films were prepared from zinc chloride $ZnCl_2$, thiourea ($SC(NH_2)_2$) and ammonium hydroxide (NH_4OH). We studied the effect of the deposition time and annealing on the growth and properties of CBD ZnS films. Trisodium citrate was used as a substitute for the hydrazine hydrate, minimizing the hazards connected with the process. The ZnS thin films deposited with using Na_3-citrate showed improved crystallinity, higher transmittance in the visible region [19]. Following various preliminary tests carried out in our laboratory, the layers prepared at deposition temperatures below 70 °C were of poor quality, non-homogeneous, non-adhering to the substrate. At higher temperatures, homogeneous precipitation in solution can take place, therefore, we had to limit the temperature of the solution to 85 °C. A typical feature of this study was the use of trisodium citrate ($C_6H_5Na_3O_7$) as a second complexing agent to deposit ZnS thin films in aqueous alkaline baths without stirring the reaction bath. Na_3-citrate is the strongest complexing agent among the non-toxic complexing agents. Obtained films were characterized for their structural, morphological electrical and optical properties by using X-ray diffraction (XRD), scanning electron microscopy (SEM), four-point probe method and optical absorption studies.

2. Experimental

2.1. Reaction mechanism

The CBD process enables deposition of thin films on substrates submerged in solutions containing chalcogenide source, metal ion, and chelating agent. The latter is used to limit the hydrolysis of the metal ion and impart some stability to the bath. The deposition rate may be controlled by adjusting temperature of the bath, pH, stirring rate and relative concentration of reactants within the solution (chalcogenide source, chelating agent and/or metal ion). Formation of ZnS film takes place when the ionic product of Zn^{2+} and S^{2-} ions exceeds the solubility product of ZnS. ZnS thin film deposition is based on the slow release of Zn^{2+} and S^{2-} ions in the chemical solutions which then condense on the glass substrate. The flow chart of the growth mechanism for the ZnS film is presented in Fig. 1.

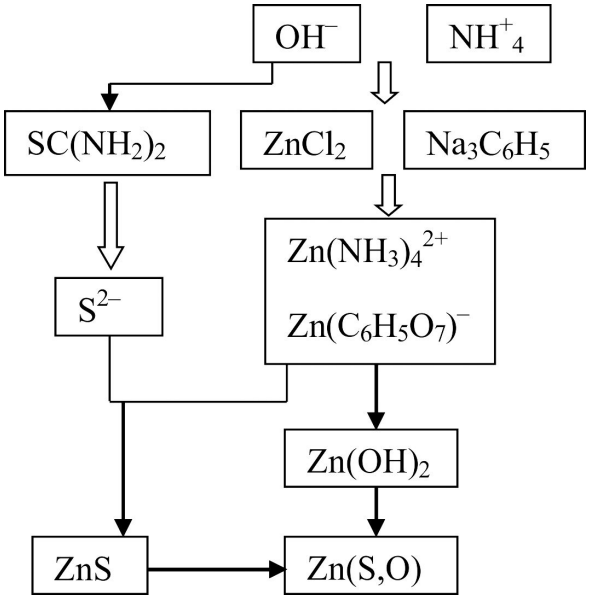

Fig. 1. Flow chart of the growth mechanism of ZnS films obtained by chemical bath deposition method.

In water solutions, zinc chloride ($ZnCl_2$) dissolves and gives Zn^{2+} ion. Also, in alkaline medium, thiourea releases S^{2-} ions. Ammonia reacts with water and gives OH^- ions. These OH^- ions form with Zn^{2+} a $Zn(NH_3)_4{}^{2+}$ complex. Therefore, suitable complexing agents should be used to limit free Zn^{2+} concentration and decrease formation of zinc hydroxide and finally zinc oxide.

Various reactions involved in the ZnS growth process can be explained by the following equations:

$$[Zn(NH_3)_n]^{2+} \leftrightarrow Zn^{2+} + nNH_3 \qquad (1)$$

$$(SC(NH_2)_2) + OH^- \leftrightarrow SH^- + CN_2H_2 + H_2O \quad (2)$$

$$SH^- + OH^- \leftrightarrow S^{2-} + H_2O \quad (3)$$

$$Zn^{2+} + S^{2-} \rightarrow ZnS \quad K = 5 \times 10^{-24} \quad (4)$$

2.2. Deposition of ZnS thin films

ZnS thin films were deposited on glass substrates by CBD technique. First of all, the substrate was cleaned in deionized (DI) water, then cleaned with methanol and acetone, again rinsed in distilled water and dried in air. The degreased substrate provided nucleation centers for the growth of the films thus giving highly adhesive and uniform films. The ZnS thin films were chemically grown on glass substrates using zinc chloride ($ZnCl_2$) as Zn^{2+} ions source, thiourea $SC(NH_2)_2$ as S^{2-} ions source [20], and ammonium hydroxide (NH_4OH) and trisodium citrate as complexing agents limiting the concentration of Zn^{2+} in the aqueous medium. In this work, each solution, i.e. precursor of cationic and anionic solution, was prepared separately. All reagents were of high analytical grade.

The films deposition was done in a reactive bath prepared in a 100 mL beaker. In the first step, 20 mL of 0.1 M of $ZnCl_2$ and 40 mL of 0.6 M solution of trisodium citrate ($C_6H_5Na_3O_7$) were mixed and stirred for 30 minutes. Then, 20 mL of 0.8 M solution of thiourea was added slowly to the mixed solution under stirring. The pH of the solution was fixed at 11 by adding a sufficient amount of 25 % ammonia solution (NH_4OH). The solution temperature was maintained at 80 °C using a thermostatic control. The glass substrates were immersed vertically inside this beaker. Fig. 2 shows the experimental setup for chemical bath deposition technique. The deposited film was prepared at water bath temperature $T_b = 80$ °C, for different durations (60 min, 90 min, 120 min and 150 min). When the deposition reactions were completed, each sample was removed from the beaker and was cleaned with deionized water and dried in air to remove the loosely adhered ZnS particles on the films. The obtained deposit was in the form of a white uniform, transparent, and well adherent film. Then, the ZnS film prepared at 80 °C for 90 min was annealed at 500 °C for 2 hours after deposition.

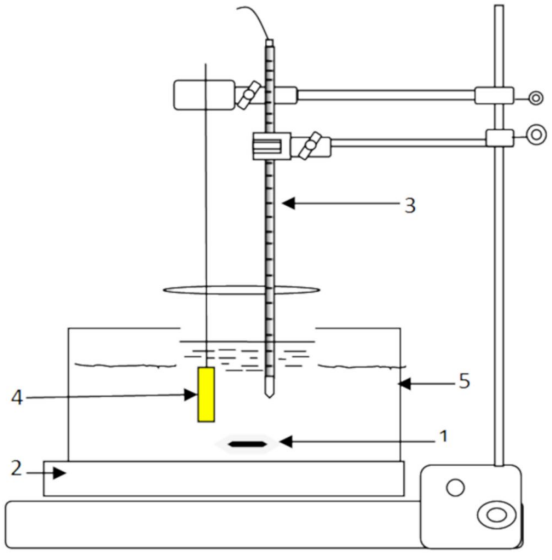

1 - Stirrer, 2 - Hot plate, 3 -Thermocouple,
4 - Substrate and 5 - Reactive aqueous solution.

Fig. 2. Experimental setup for chemical bath deposition of thin film.

The obtained film thickness was estimated from a stylus displacement of a Dektak profilometer. The transmittance spectrum of ZnS thin film was recorded by UV-Vis (Shimadzu UV-3101) spectrophotometer in the range of 300 nm to 800 nm. The X-ray diffraction (XRD) patterns of the film were recorded using a PHILIPS PW 3710 diffractometer operating at 40 kV, 20 mA and $\lambda_{CuK\alpha} = 1.54$ Å. The surface morphology of the films was measured by scanning electron microscopy (SEM). Infrared spectrum of the film deposited on silicon substrate was recorded using Fourier Transform infrared spectrophotometer and the composition of the film was obtained by energy-dispersive X-ray spectroscopy. The electrical conductivity was measured at room temperature via the four-point probe method, using a JANDEL RM 3000 device.

3. Results and discussion

3.1. Thin films growth

In order to explain the influence of deposition time on the formation of ZnS films, the films were deposited at various deposition times namely 60 min, 90 min, 120 min and 150 min. The variation of ZnS film deposition rate as a function of time is shown in Fig. 3. It seems clear that the deposition rate depends on deposition time. At the beginning of the deposition process, the rate of growth is decreasing as a function of time. It is relatively high at the beginning of the deposition process due to the increase of nucleation centers and becomes progressively lower thereafter. However, the solution heating causes a decrease in the concentration of NH_3, therefore, NH_3 has not reacted completely with Zn^{2+} ions, and free Zn^{2+} ions remained in the reaction bath, where $Zn(OH)_2$ could be easily precipitated in the basic solution resulting in low concentration of ZnS. The relatively low concentration of ZnS ions in the bath resulted in a low growth rate. On the other hand, from a certain deposition time, the thickness increases rapidly, leading to an increase in the growth rate of the films. The time of changing the behavior is equal to 90 min. This growth can be explained by the contribution of the homogeneous regime (appearance of particles in the solution). This regime induces an increase in the growth rate of ZnS in thin layer by direct adsorption of ZnS clusters found in the solution.

In Fig. 3, the ZnS film prepared at 80 °C for 150 min shows a maximum film growth rate (about 4.08 nm/min).

3.2. Structural properties

Fig. 4 shows X-ray diffraction patterns of the deposited films for the four deposition times considered in this work. As we can see, ZnS phase with the cubic structure and preferred orientation along (2 0 0) plane has been obtained after 90 min, as it has been reported in the literature [21, 22]. Similar (2 0 0) plane dominance was also reported by Liang et al. [23], for ZnS films prepared by cathodic electrodeposition technique. A maximum intensity of the (2 0 0) peak was noticed for the layer deposited at 90 min.

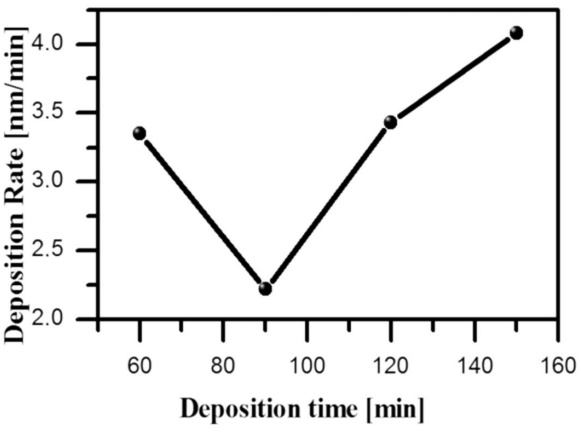

Fig. 3. Deposition rate of ZnS thin films at different deposition times.

As it can be inferred from the XRD patterns, the film deposited for 60 min seems to be amorphous. The (2 0 0) peak is lightly shifted to lower diffraction angles with a noticeable reduction in its intensity when the deposition time equals 150 min, and on the other hand, an increase in the intensity of (2 2 0) peak is observed. The films deposited during 120 min, show only one preferential orientation along (2 2 0) direction at $2\theta = 47.29°$ indicating a cubic structure. Thus, the XRD patterns depend strongly on deposition time. The grains sizes were found to be ranged from 162.1 nm to 154.5 nm as the deposition time was changed from 90 min to 150 min.

The grain size D of the deposited films can be determined by using Scherer equation [40]:

$$D = \frac{K\lambda}{\beta \cos\theta} \tag{5}$$

where K is approximately equal to 0.94, $\lambda = 1.54184$ Å, θ is the diffraction angle and β is the width of diffraction line at half maximum intensity.

The microstrain ε of the films was estimated using the equations [41]:

$$\varepsilon = \frac{\beta \cos\theta}{4} \tag{6}$$

The values of structural parameters: average grain size D, microstrain ε for ZnS thin films

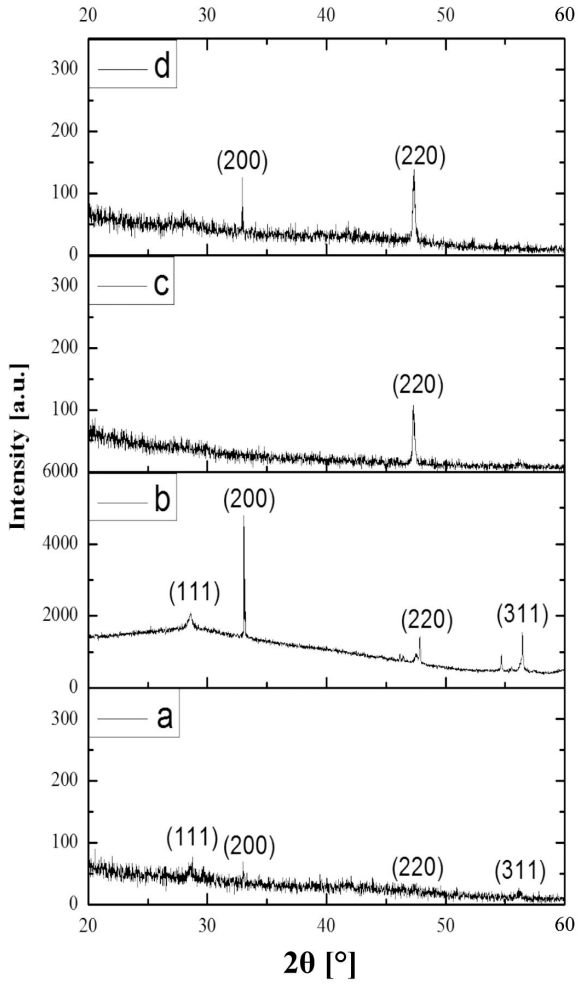

Fig. 4. X-ray diffraction patterns of ZnS thin films deposited at different deposition times: (a) 60 min; (b) 90 min; (c) 120 min; (d) 150 min, on n-Si substrate.

obtained at different deposition times are presented in Table 1.

Table 1 shows the crystallite size of the layers obtained at different deposition times. The reduction of the grain size with the increase of deposition time may be due to the deterioration of the film crystallinity which may be caused by an increase of defect density in the film network, enabling the rise of internal strain in the formed crystallites.

3.3. Scanning electron microscopy (SEM)

Scanning electron microscopy (SEM) is a suitable technique to study the microstructure of thin films. This technique allows one to specify the mode of growth via the study of a surface roughness and to determine the effect of different deposition times on the film morphology. Fig. 5 shows the surface morphology of ZnS thin films deposited at temperature 80 °C, at different deposition times, observed by SEM. From the micrographs, it is observed that the as-deposited films have uniform morphology with good surface coverage (ion-by-ion mechanism) on which freely adherent clusters of grains (cluster-by-cluster mechanism) exist. The ZnS thin films have the surface structure consisting of various small particles free of pinholes. When the deposition time increases, the particle size increases from around 10 nm to 20 nm. We can conclude that the homogeneity, grain size and adhesion to the substrate can be increased by increasing deposition time.

We have estimated from the SEM images that the grain size of the films, as a function of deposition time, evolves as it is presented in Table 2.

Chemical composition of ZnS thin films on glass substrate was analyzed by energy-dispersive X-ray analyzer (EDX) (Fig. 6). The EDX analysis confirms the presence of zinc and sulfur in the ZnS thin films. We see that the percentage of sulfur is low in the film and it is probably due to the volatility of sulfur. Excess of Zn may be caused by the amount of $Zn(OH)_2$ or ZnO originating from the alkaline reaction solution. In the analysis, the presence of the peaks of O, Si, Mg, Cl and Na can be attributed to the amorphous nature of the glass substrate.

Nakada et al. [26] suggested that oxygen atoms in the ZnS film deposited by CBD method might come from the compounds of ZnO and $Zn(OH)_2$.

3.4. Optical properties

Optical properties of ZnS thin films were determined from the variation of optical transmission with UV-Vis light wavelength λ ranging from 300 nm to 800 nm.

Transmittance

Fig. 7 shows optical transmission spectra of ZnS thin films obtained at different deposition

Table 1. Structural parameters of chemically deposited ZnS thin films at different deposition times on n-Si substrate.

Deposition time [min]	(h k l)	2θ [°]	FWHM [°]	D [nm]	$\varepsilon \times 10^{-4}$
90	(2 0 0)	33.0785	0.0530	162.1	2.22
150	(2 0 0)	32.92	0.056	154.5	2.34

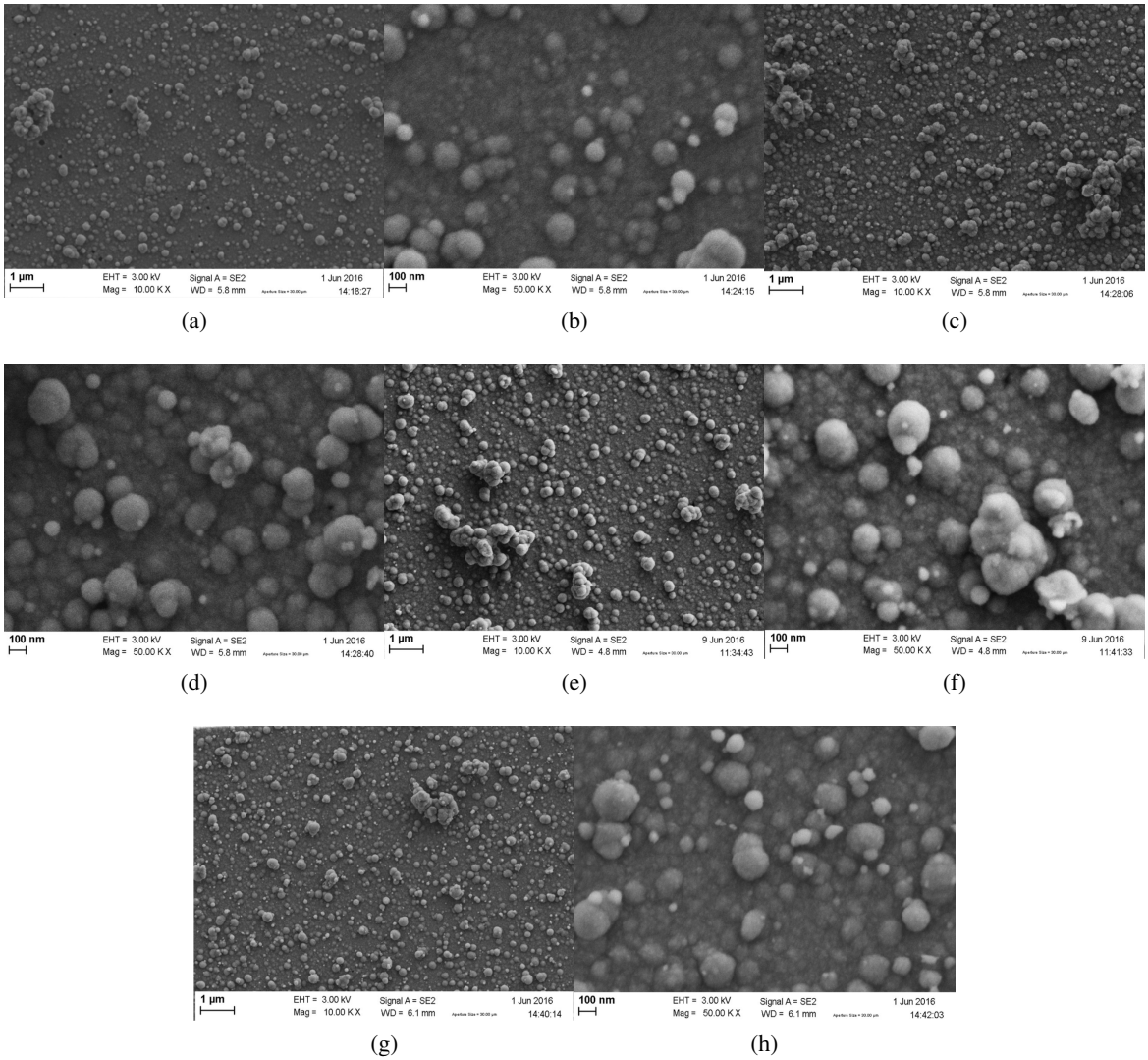

Fig. 5. SEM images of ZnS thin films deposited at various periods of time: (a) 60 min, (c) 90 min, (e) 120 min, (g) 150 min, (b, d, f, h) the images of a, c, e, g at higher magnification.

times, before and after annealing at 500 °C for 2 hours.

It is clear that the transmittance decreases with increase of deposition time, before as well as after annealing. This decrease in transmittance can be explained by the evolution of thickness, in other words, increasing the deposition time leads to thicker films. It has been observed that the as-deposited films have a maximum transmittance of 81.7 % in the visible region, which is significantly better than that reported by many authors [24, 25]. This high transparency in the visible region indicates that no colloidal particles have been formed by homogeneous reaction on the substrate surface.

Table 2. Mean ZnS grain size deduced from SEM as a function of deposition time.

SEM image	Deposition time[min]	Grains size [nm]
Fig. 4a	60	10
Fig. 4c	90	17
Fig. 4e	120	22
Fig. 4g	150	20

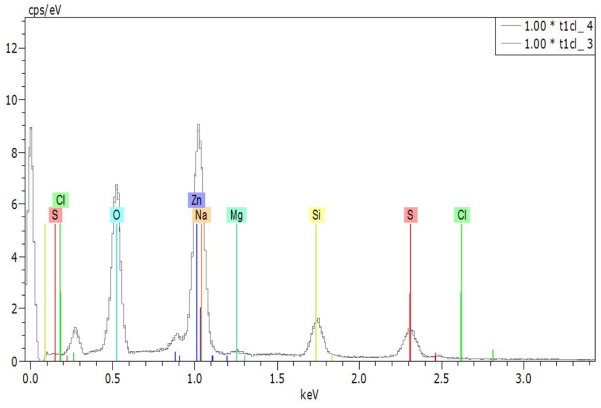

Fig. 6. EDX scanning pattern of ZnS layer deposited at 80 °C for 60 min.

This result is in agreement with SEM micrographs. The average transmittance in the visible range of the film deposited for 90 min and annealed at 500 °C for 2 h is about 87.4 %, which is higher than of that deposited at 150 min. Annealing process of the as-deposited films increases the optical transmittance. This increase could be attributed to the rearrangement and decrease of the films defects. Furthermore, we notice the absence of interference fringes that may be due to the multiple reflections on the interfaces film/substrate and film/air. Therefore, the absence of these fringes in our films indicates a roughness of the surface of ZnS films, which causes scattering of incident light on the material.

Absorbance and reflectance

Fig. 8 and Fig. 9 show spectral variations of the reflectance and absorbance for as-deposited and annealed films. It can be seen that all the samples of ZnS films exhibit high absorbance in UV regions. In the visible region, the absorbance is low. Also, the values for the annealed film are lower

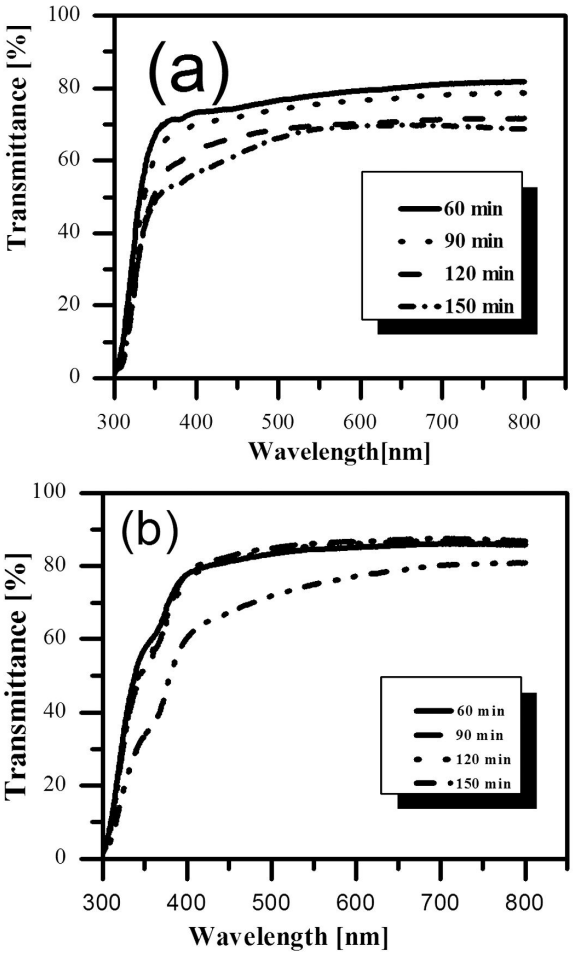

Fig. 7. Transmittance spectra of ZnS films grown on glass substrate at various deposition times: (a) as-deposited, (b) annealed at 500 °C for 2 h.

compared with the others because the annealed film has a higher transmittance values.

Absorption coefficient and optical band gap

The α coefficients for as-deposited and annealed ZnS films were calculated by the following relationship [28]:

$$\alpha = 2.3026\ \mathrm{A/t} \qquad (7)$$

where A is the absorbance and t is the sample thickness.

In Fig. 10, the variation of α versus wavelength for ZnS nanocrystalline thin layers with deposition time as parameter is reported. One can clearly see that the absorption coefficient of the ZnS films increases with the decrease of wavelength.

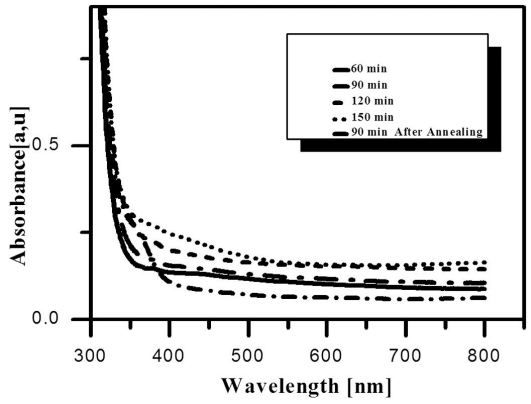

Fig. 8. Optical absorbance of nanocrystalline ZnS thin films obtained at different deposition times versus wavelength before and after annealing.

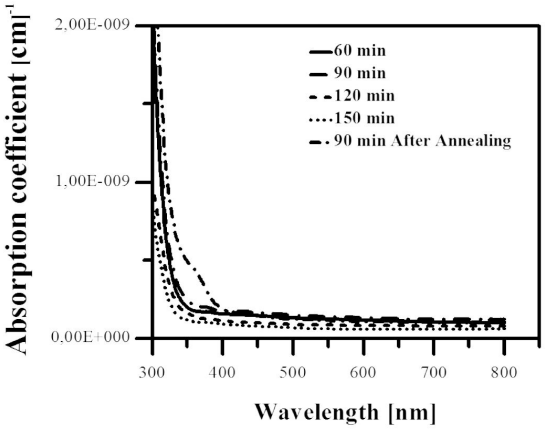

Fig. 10. Absorption coefficient of ZnS thin films obtained at different deposition times versus wavelength before and after annealing.

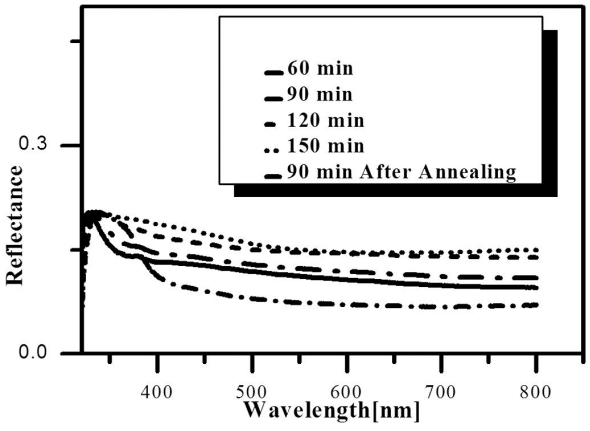

Fig. 9. Optical reflectance of nanocrystalline ZnS thin films obtained at different deposition times versus wavelength before and after annealing.

The absorption coefficient values were used to determine the optical energy gap by using the Tauc relationship which is given by the formula [29]:

$$\alpha h\nu = \beta(h\nu - E_g)^n \tag{8}$$

in which, hν is the photon energy, E_g is the optical band gap of the semiconductor, β is a constant and n = 1/2 for direct band gap semiconductor such as ZnS. The optical band gap value of the ZnS thin films was estimated by extrapolation of the straight line of the plot of $(\alpha h\nu)^2$ versus photon energy as it is shown in Fig. 11. We found that the E_g value for the films prepared at different deposition times varies from 3.78 eV to 4.03 eV, which is in agreement with what has been reported by other authors [27].

According to Fig. 11, the bandgap energy of the ZnS thin films first decreased from 4.03 eV to 3.87 eV in deposition time range of 60 min to 120 min. This band gap reduction was caused by the increase in film thickness owing to increased crystallite size [30]. However, after that, the optical gap increased from 3.87 eV to 3.96 eV with the increasing deposition time, which can be explained by the decrease in the disorder. This may also be due to the presence of zinc hydroxide produced by the alkaline bath, thereby, forming a mixture of zinc sulfur hydroxide Zn(S,OH) [31]. It is clear from Fig. 11 that the gap energy values of the films before annealing are greater than those after annealing. The decrease in the film band gap width after annealing could be attributed to improvement in the crystal structure and grain sizes change of the films. This result is in good agreement with the reported one by others authors [32]. Table 3 shows the results of the optical energy gap calculation for ZnS thin films before and after annealing [34].

Urbach energy or band tail width

The relationship between α and hν is known as Urbach empirical rule, which is given by the following exponential equation [42]:

$$\ln(\alpha) = \ln(\alpha_0) + \left(\frac{h\nu}{E_{00}}\right) \tag{9}$$

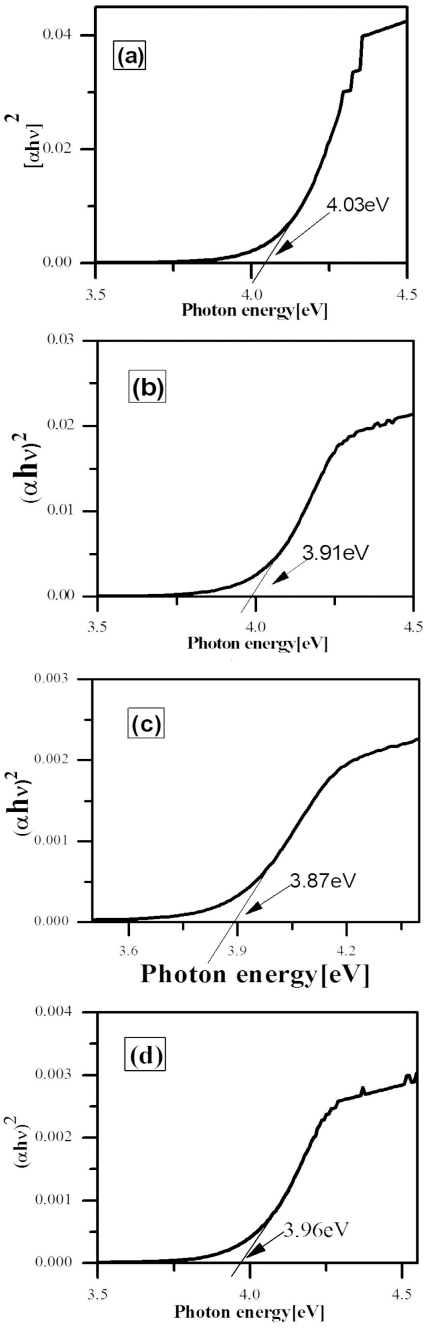

Fig. 11. The plot of $(\alpha h\nu)^2$ versus photon energy ($h\nu$) for ZnS thin films prepared at various deposition times: (a) 60 min; (b) 90 min; (c) 120 min; (d) 150 min.

where α_0 is a constant, $h\nu$ is the incident photon energy and E_{00} is the band tail width (Urbach energy) of the localized states in the optical energy gap.

Table 3. Gap energy values of ZnS thin films before and after annealing.

Deposition time[min]	Direct band gap energy Eg [eV]	
	Before annealing	After annealing
60	4.03	–
90	3.91	3.83
120	3.87	–
150	3.96	–

The tail width E_{00} in the gap energy was obtained by plotting $\ln\alpha$ as a function of $h\nu$. The inverse of the slope extracted from the linear part gives E_{00} for the deposited ZnS films, as shown in Fig. 12. The E_{00} value increases with increasing of deposition time until it reaches the value of 120 min after which the tail width decreases. The time of change of the behavior is equal to 120 min which corresponds to the maximum disorder (ion mixed growth regime by ion and cluster by cluster). As can be seen, the variation of optical gap value is opposite to the disorder. This behavior indicates clearly that the optical gap is also controlled by disorder in the film.

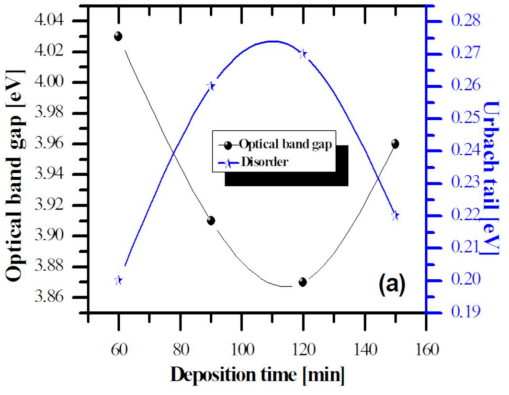

Fig. 12. Optical gap and disorder variations of CBD-ZnS thin films as a function of deposition time.

Extinction coefficient k

The extinction coefficient k is estimated from the following equation [33]:

$$k = \alpha\lambda/4\pi \tag{10}$$

where λ is the incident radiation wavelength.

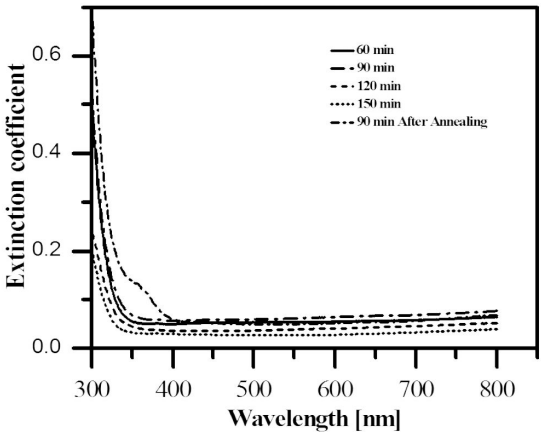

Fig. 13. Extinction coefficient of nanocrystalline ZnS thin films obtained at different deposition times versus wavelength, before and after annealing.

Fig. 13 shows the evolution of the extinction coefficient as a function of wavelength for different deposition times of ZnS films. The extinction coefficient decreases as the wavelength increases and moreover it increases when the deposition time increases. This decrease in extinction coefficient may be the result of increased surface roughness, as the film thickness increase induces the increase in surface optical scattering and extinction coefficient. Fig. 13, shows also the extinction coefficient of the sample annealed at 500 °C for 120 min. From this figure, it can be inferred that the annealing process leads to decrease in the extinction coefficient. This might be caused by the fact that the annealing process minimizes the defects or the tail depth (which means decreasing in the film absorbance).

Refractive index n

The refractive index is determined from transmittance spectra, as a function of wavelength, using a simple approximated relationship [35]:

$$n = \frac{1+R}{1-R} + \left[\frac{4R}{(1-R)^2} - k^2\right]^{1/2} \qquad (11)$$

where R is the reflectance for any intermediate energy photon recorded by spectrophotometer, and k the extinction coefficient.

The refractive index variations in the wavelength range of 300 nm to 800 nm, for different deposition times, are shown in Fig. 14. It is seen that the refractive index increases with increasing the deposition time in the range of 60 min to 150 min. This may be due to the film thickness increase and the formation of non-stoichiometric oxide phases in the ZnS films [36].

The figure also shows the effect of annealing process on the refractive index. It is clear that the annealing process induces a decrease in the refractive index values. After annealing, the refractive index of the films is reduced by about 10 % in the visible range. This decrease is attributed to the fact that ZnS film surface begins to be oxidized when the film is annealed at 500 °C.

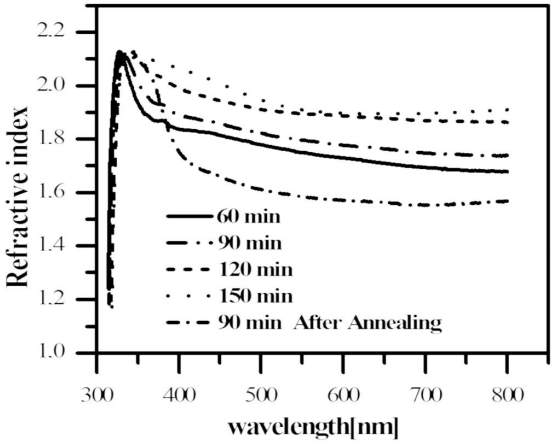

Fig. 14. Refractive index of nanocrystalline ZnS thin films obtained at different deposition times versus wavelength, before and after annealing.

Moreover, FT-IR studies were used to verify the presence of ZnS and other impurities present on the surface of the films.

Fig. 15 shows the measured FT-IR spectra of the films of ZnS deposited at different deposition times on glass and monocrystalline silicon substrates. The absorption band located at 615 cm^{-1} can be attributed to the formation of ZnS phase [37]. The spectra show a large peak centered at 3360 cm^{-1} and a small peak at 1630 cm^{-1}, which are due to stretching and bending modes of H–OH. This might be due to trace amount of adsorbed water present on the film surface. The spectra show a small peak at 1110 cm^{-1} which is assigned to stretching mode of Zn–OH. The spectra also show a weak band in the region of 1475 cm^{-1}, which

could be due to the bending modes of C–H. Based on this study, we can say, the film contains some amount of $Zn(OH)_2$.

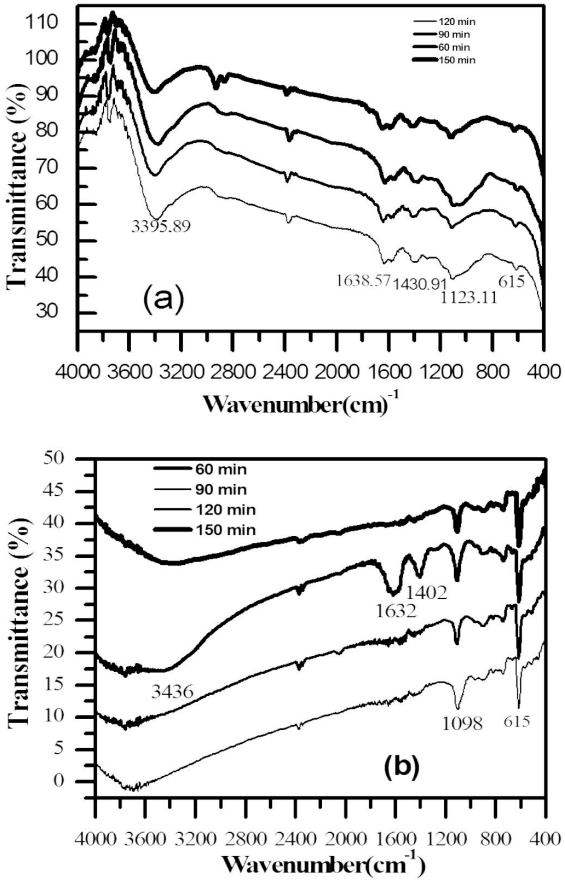

Fig. 15. Vertically shifted FT-IR spectra of a typical ZnS film deposited at different deposition times, (a) on glass, (b) on monocrystalline Si substrate.

3.5. Electrical properties

The resistivity of our ZnS thin films was calculated according to equation 12 [39]:

$$\rho = R_S \cdot d \tag{12}$$

where ρ is the resistivity, R_S is the square resistance ($R_S = \frac{\pi}{\ln 2} \cdot \frac{U}{I}$, U is the voltage and I is the current) and d is the film thickness. The evolution of the electrical conductivity as a function of the deposition time is shown in Fig. 16.

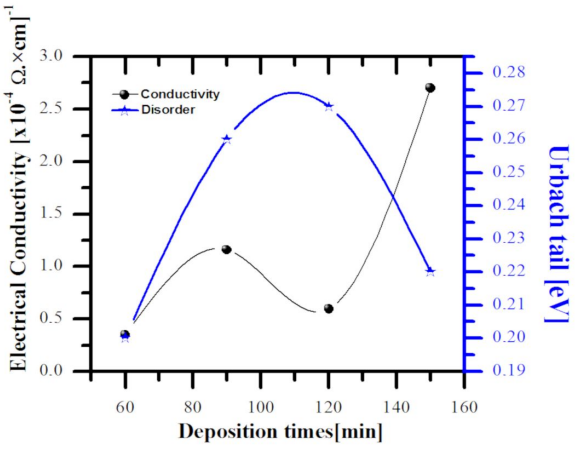

Fig. 16. Variation of electrical conductivity and disorder of the ZnS thin films deposited at different deposition times.

In this figure, we note that the electrical conductivity of the ZnS films increases from 0.35×10^{-4} Ω·cm^{-1} to 2.7×10^{-4} Ω·cm^{-1} with increasing of deposition time. The increase in conductivity with the deposition time is due to the increase in film thickness. Indeed, structural defects in thin films are reduced with thickness, which explains the increase in conductivity [38]. In the same figure, we can also observe an increase in conductivity with a decrease in disorder in the films. In general, the increase in conductivity is a consequence of the decrease in disorder. Moreover, the decreasing of the conductivity at t = 120 min is attributed to the phenomenon of oxygen absorption, which could play the role of accepting impurities.

4. Conclusions

Economical chemical bath deposition (CBD) technique was used to deposit ZnS thin films with high transparency. Thin films of zinc sulfide were deposited onto glass substrates from the aqueous solution of zinc chloride, ammonia solution, thiourea and trisodium citrate ($Na_3C_6H_5O_7$), wherein the Na_3-citrate was used as non-toxic complexing agent. The effect of deposition time was investigated. The thickness of ZnS films increased nearly linearly with time after the nucleation phase (ca. 90 min). The X-ray diffraction analysis

revealed a cubic structure of the ZnS thin films. The SEM images demonstrated a dense and uniform surface that was free of pits or pinholes. The fine grains with different sizes, uniformly distributed on the smooth and homogeneous surface, were well defined and spherical in shape. The films exhibited also good adherence and covered the entire substrate surface. The EDX analysis confirmed the presence of zinc and sulfur in the ZnS thin films.

The optical properties of the as-deposited films and the films annealed at 500 °C for 120 min were studied. The films were highly transparent. The percentage of transmission was around 82 % for all the as-deposited ZnS films in the visible range, while for the annealed films, the percentages exceeded 82 %, except for the film deposited for 150 min. The measured band gap was found to be in the range of 3.87 eV to 4.03 eV depending upon the deposition time. These results indicate that ZnS films are suitable for use as the buffer layer in Cu(In, Ga)Se_2 solar cells.

References

[1] HASSANIEN A.S., AKL A.A., *Superlattice. Microstruct*, 89 (2016), 153.

[2] HUANG Y.-H., JIE W.-Q., ZHOU Y., ZHA G.-Q., *J. Alloy. Compd*, 549 (2013), 184.

[3] DÍAZ REYE S.J., CASTILLOOJEDA R.S., SÁNCHEZES PÍNDOL A. R., *curr. Appl*, 15(2015), 103.

[4] CHA J.H., KWON S.M., BAE J.A., YANG S.H., JEON C.W., *J. Alloy. Compd*, 708 (2017),562 .

[5] LEI Y., CHEN F.F., LI R., XU J., *Appl. Surf. Sci*, 308 (2014), 206.

[6] PIQUETTE E.C., BANDIC Z.Z., MCCALDIN J.O., MCGILL T.C., *J. Vac. Sci. Technol. B,* (1997).

[7] KURBATOV D., KSHNYAKINA S., OPANASYUK A., MELNIK V., NESPRAVA V., *Rom. J. Phys.*, 55 (2010), 213.

[8] BOSCO J.P., DEMERS S.B., KIMBALL G.M., LEWIS N.S., *J. Appl. Phys,* 9 (2012).

[9] WU X., LAI F., LIN L., LVJ., ZHUANG B., YAN Q., HUANG Z., *Appl. Surf. Sci.,* 254 (2008), 6455.

[10] XU G., MIAO C., LIU G., YE C., *J. Mater. Chem.*,11 (2012), 4890.

[11] LIU T.Z., KE H., ZHANG H., *Mater. Sci. Semicond. Proc.*, 26 (2014), 301.

[12] KHALIFA Z.S., MAHMOUD S.A., *Physica E*, 60 (2017), 91.

[13] BHALERAO B.A., LOKHANDE D.C., WAGH G.B., *Nanotechnol.*,6 (2013), 996.

[14] KRIISA M., KIIRBER E., KRUNKS M., *Thin Solid Films*, 87 (2014), 555.

[15] HAUBI N.F., MIDHJIL K.A., RASHID H.G., MANSOUR H., *Phys. Lett.*,24 (2010).

[16] SULTANA J., PAUL S., KARMAKAR A., YI R., DALAPATI G.K., CHATTOPADHYAY S., *Appl. Surf. Sci.*, 418 (2017), 380.

[17] LIU J., WEI A., ZHAO Y., *J. Alloy.Compd.*, 588 (2014), 228.

[18] HARISKOS D., SPIERING S., POWALLA M., *Thin Solid Films*, 480(2005), 99.

[19] WOOK S.S., AGAWANE G.L., MYENG G.G., MOHOLKAR A.V., *J. Alloy. Compd.*, (2012), 25.

[20] SHIN S.W., AGAWANE G.L., GANGB M.G., MOHOLKARC A.V., MOON J.H., KIM J.H., LEE J.Y., *J. Alloy. Compd.*, 526 (2012).

[21] KASSIMA., NAGALINGAM S., *Arabian J. Chem.*, 249 (2010), 234.

[22] DUBROVIN. I.V., BUDENNAYA L.D., MIZETSKAYA I.B., SHARKINA, *Inorg. Mater.*, 19 (1983), 1603.

[23] LIANG G., FAN P., CHENC., LUO J., ZHAO J., ZHANG D., *Mater. Electron.*, 26 (2015), 2230.

[24] OZKAN M., EKEM N., PAT S., BALBA M.Z., *Mater. Sci. Semicond. Proc.,* 15 (2012), 113.

[25] LADAR M., POPOVICI E.J., BALDEA I., GRECU R., *J. Alloy. Compd.*, 434 (2007), 697.

[26] NAKADA T., FURUMI K., KUNIOKA A., *IEEE Trans. Elec. Dev.,* 46 (1999) 2093.

[27] KANG S.R., SHIN S.W., CHOI D.S., MOHOLKAR A.V., MOON J.H., KIM J.H., *Curr. Appl. Phys,* 10 (2010), 437.

[28] SINGH J., *John. Wiley. Sons*, (2006).

[29] NIEN Y.T., CHEN I.G., *J. Alloy. Compd.,* 471 (2009), 553.

[30] OBAID A.S., MAHDI M.A., AHMED DIHE A., HASSAN Z., *Appl. Sci. Manag.*, 2012 (2012), 26.

[31] LOKHANDE C.D., PATIL P.S., TRIBUTSCH H., ENNAOUI A., *Sol. Eng. Mat. Sol. C.*, 55 (1998), 379.

[32] KE H., DUO S., LIU T., SUN Q., RUAN C., FEI X., TANJ, ZHAN S., *Mater. Sci. Semicond. Proc.,* 18 (2014), 28.

[33] FATHY N., KOBAYASHI R., ICHIMURA M., *Mater. Sci. Eng. B*, 107 (2004), 271.

[34] OFFIAH S.U., UGWOKE P.E., EKWEALOR A.B., EZUGWU S.C., OSUJI R.U., EZEMA F.I., *Digest. J. Nanomater. Biostruct.*, 7 (2012), 165.

[35] BREWE RS. H., FRANZEN S., *J. Alloy. Compd.*, 338 (2002), 73.

[36] ARENA O.L., NAIR M.T.S., NAIR P.K., *Semicond. Sci. Technol.*, 12 (1997), 1323.

[37] YANG H., ZHAO J., SONG L., *Mater. Lett*, 15 (2003), 2287.

[38] KULKANI D., *Bull. Mater. Sci.*, 28 (2005), 43.

[39] DERBALIA A., SAIDIA H., ATTAFA A., BENAMRAAH., BOUHDJERA A., ATTAFBN., EZZAOUIAC H., *J. Semicond*, 9 (2018), 45.

[40] BENDJEDIDI H., ATTAF A., SAIDI H., AIDA M.S., SEMMARI S.,BOUHDJAR A., BENKHETTA Y., *J. Semicond.*, 36 (2015), 12.

[41] AKL A.A., MAHMOUD S.A., AL-SHOMAR S.M., HASSANIEN A.S., *Mater. Sci. Semicond. Proc.*, 74 (2018), 183.
[42] HASSANIEN A.S., AKL A.A., *J. Alloy. Compd*,. 648 (2015), 280.

Received 2018-05-12
Accepted 2018-10-10